

Random projections in gravitational wave searches of compact binaries

Sumeet Kulkarni,¹ Khun Sang Phukon,² Amit Reza,³ Sukanta Bose,^{4,5}
Anirban Dasgupta,³ Dilip Krishnaswamy,⁶ and Anand S. Sengupta³

¹*Indian Institute of Science Education and Research, Homi Bhabha Road, Pune 411008, India*

²*Department of Physics, Indian Institute of Technology, Kanpur 208016, India*

³*Indian Institute of Technology Gandhinagar, Gujarat 382355, India*

⁴*Inter-University Centre for Astronomy and Astrophysics, Post Bag 4, Ganeshkhind, Pune 411 007, India*

⁵*Department of Physics & Astronomy, Washington State University, 1245 Webster, Pullman, WA 99164-2814, U.S.A.*

⁶*IBM Research, Bangalore 560045, India*

Random projection (RP) is a powerful dimension reduction technique widely used in analysis of high dimensional data. We demonstrate how this technique can be used to improve the computational efficiency of gravitational wave searches from compact binaries of neutron stars or black holes. Improvements in low-frequency response and bandwidth due to detector hardware upgrades pose a data analysis challenge in the advanced LIGO era as they result in increased redundancy in template databases and longer templates due to higher number of signal cycles in band. The RP-based methods presented here address both these issues within the same broad framework. We first use RP for an efficient, singular value decomposition inspired template matrix factorization and develop a geometric intuition for why this approach works. We then use RP to calculate approximate time-domain correlations in a lower dimensional vector space. For searches over parameters corresponding to non-spinning binaries with a neutron star and a black hole, a combination of the two methods can reduce the total on-line computational cost by an order of magnitude over a nominal baseline. This can, in turn, help free-up computational resources needed to go beyond current spin-aligned searches to more complex ones involving generically spinning waveforms.

I. INTRODUCTION

The direct detections of gravitational waves (GWs) from the mergers of black holes and neutron stars [1–6] by Advanced LIGO (aLIGO) [7] and Advanced Virgo (AdV) [8] detectors in the first and second observing runs (O1 and O2, respectively) have launched the era of GW astronomy [9, 10]. In the coming years, the global network of ground-based detectors, comprising aLIGO, AdV, KAGRA [11] and LIGO-India [12] will not only increase the detection rate and facilitate the search for their possible electromagnetic counterparts [13–15] but also produce an unprecedentedly large amount of data, which can pose an interesting computational challenge for GW data analysis.

At present, theoretically modeled compact binary coalescence (CBC) waveforms are used as templates to *matched-filter* [16] the detector data in these searches [17, 18]. A brute force computation of this cross-correlation with a suitable grid of templates spanning astrophysical ranges of search parameters can be expensive (but see [19–21]). As these detectors are paced through planned upgrades, one expects better sensitivity at low frequencies and an increase in the detector bandwidth. The combined effects of these changes will not only increase the volume of the search parameter space but also result in denser template banks, thereby increasing their redundancy. More cycles of the signal will fall in band and increasing their duration. These highlight the need for designing efficient and scalable methods for matched-filtering-based templated CBC searches [22–27].

In a seminal work, Cannon *et al.* [28–30] showed

how singular value decomposition (SVD) can mitigate the redundancies in CBC template banks by effectively reducing the number of filters or templates, owing to their strong correlation for similar parameter values, with negligible effect on search performance. We show, however, that the computational cost of SVD factorization does not scale favorably with increase in bank size. Further, it may not be possible to factorize very large banks *in toto* as it requires prohibitively large random access memory.

Random Projections (RP), conceived by the pioneering work of Johnson and Lindenstrauss [31], is a computationally efficient technique for dimension reduction and finds applications in many areas of data science [32]. In this *Letter*, we apply this technique to address two key challenges in future CBC searches: handling redundancies in large template databases; and efficiently correlating noisy data against long templates.

The *primary impact* of this work is multi-fold: (1) Efficient template matrix factorization can be used to address the *redundancy problem*. This is similar in spirit to the SVD factorization that is at the heart of the “GstLAL”-based inspiral pipeline [27, 30, 33], but our RP method scales well for very large number of templates embedded in high-dimensional Euclidean space. Such factorizations can be done off-line, in advance of a CBC search. Nonetheless there can be situations when the factors need to be updated on-line, e.g., owing to the non-stationarity of data. Our adaptations will benefit both scenarios. (2) We show the explicit connection between the new factorization scheme and the extant SVD method. This bridges

the two approaches and makes it readily usable. (3) The computational challenges arising from correlating noisy data against long templates (also known as the *curse of dimensionality*) is addressed by casting the matched-filtering operation in a lower-dimensional space. For certain types of template banks (e.g., for CBCs with precessing spins), the template matrix may be less amenable to a SVD-like factorization. There the total computational cost can be significantly reduced by using the RP-based correlation alone. (4) Finally, we show that RP-based template matrix factorization and matched-filtering computation in reduced dimension can be combined effectively for efficient CBC searches.

Currently the GstLAL-based inspiral pipeline utilizes time-slicing of templates to improve computational efficiency, and also involves spin-aligned templates. Since it is for the first time that the RP is being introduced in GW searches, our primary objective here is to elucidate how its core ideas can help them. This is why we demonstrate application of RP in the simple case of a single slice of data and non-spinning inspiral templates. This simplification notwithstanding, the RP-based methods introduced here can be readily applied to time-sliced data and spin-aligned templates. (A detailed study of that application and the computational advantage so gained will be presented in a future work.)

II. COMPACT BINARY SEARCHES

Consider a CBC search involving a bank of N_T templates over a given parameter space. Following the convention in Ref. [28], let \mathbf{H} denote the $2N_T \times N_s$ *template matrix* with $2N_T$ rows of real-valued unit-norm whitened filters, each sampled over N_s time-points. The template matrix may be viewed as $2N_T$ row-vectors embedded in N_s -dimensional Euclidean space \mathbb{R}^{N_s} . The complex matched-filter output of the α^{th} template at a specific point in time, against the whitened data \vec{S} is the inner product:

$$\rho_\alpha = (H_{(2\alpha-1)} - iH_{(2\alpha)}) \vec{S}^T, \quad (1)$$

where H_α denotes the α^{th} row of \mathbf{H} and \vec{S}^T is the transpose of \vec{S} . The signal-to-noise ratio maximized over the initial phase ϕ_0 , is given by $|\rho_\alpha|$. In our notation, the H_α 's and signal \vec{S} are assumed to be row vectors. The overlap between two templates, when maximized over *extrinsic* parameters (e.g., the time t_0 and phase ϕ_0 at arrival or coalescence of the signal in band), produces the *match*. The match between templates with similar intrinsic parameters (such as the compact object masses and spins), can be very high - signifying the rank deficiency of the template matrix. A typical *off-line* CBC search involves calculating the cross-correlation between \vec{S} and every row of \mathbf{H} for a series of relative time-shifts, or values of t_0 , thereby

generating a time-series of ρ_α values, for every α . The use of a large number of templates (N_T), each sampled over a large number of points (N_s) amplifies the search's computational cost.

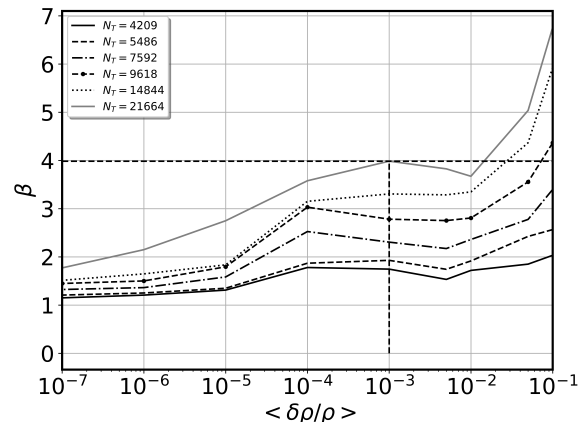


FIG. 1. The factor by which the number of SVD basis vectors increases due to partitioning of template bank of size N_T into sub-banks of 500 templates each is shown as β on the vertical axis. Results from five different template-bank sizes are shown. As one approaches machine-precision accuracy in SNR reconstruction, $\beta \rightarrow 1$ as expected. A practical operating point would be $\langle \delta\rho/\rho \rangle \sim 10^{-3}$. The trend from the five examples shown here indicates that β can be quite large for searches in aLIGO data where $N_T \sim 10^5$.

The rank deficiency of \mathbf{H} is exploited in the truncated SVD approach, where every row is approximated as a linear combination of only ℓ of the $2N_T$ right singular vectors with the most dominant singular values. Further, these “basis” vectors are used as eigen-templates against which the data are cross-correlated. The left singular vectors of \mathbf{H} and the singular values are combined into a coefficient matrix that is used to reconstruct the approximate signal-to-noise ratio (SNR). The truncation of the basis leads to errors in the approximation of the template waveforms, which further translates to imperfect reconstructions of the SNR. The fractional SNR loss can be measured as a function of the discarded $(2N_T - \ell)$ singular values.

The SVD factorization of the template matrix \mathbf{H} has a time-complexity proportional to $\mathcal{O}(N_T^2 N_s)$ assuming $N_T \leq N_s$. Thus, such factorizations fast become computationally unviable with increasing size of a template bank. Since the entire template matrix can become too large to be saved in single machine memory, a suitable parallel scheme is required to apply SVD to larger banks. SVD-based on-line CBC searches [33, 34] work around this problem by splitting the bank into smaller sub-banks that are more amenable to such factorization separately. While the optimal way of partitioning the bank is an open problem, the act of splitting the bank prevents exploitation of the *linear dependency* of templates across the sub-banks. This is

seen in Fig. 1, where we plot β , which is defined as the ratio of the number of basis vectors summed across all the sub-banks to the number of basis vectors from the SVD factorization of the full bank, at a given average fractional loss in accuracy of the reconstructed SNR. By splitting the bank, one effectively ends up requiring many more eigen-templates against which the data are filtered.

The SVD-inspired RP-based factorization presented below addresses this issue and is scalable for large template banks. We also apply RP to calculate the correlations in a lower-dimensional space \mathbb{R}^k where $k \leq N_s$. These correlations could be either between a template and the data as shown in Eq. (1) or between the basis vectors and the data within the SVD paradigm. The full potential of the RP-based methods introduced here can be realized by combining them together. We demonstrate its feasibility with an example.

III. RANDOM PROJECTION

The core theoretical idea behind the RP technique is the Johnson-Lindenstrauss (JL) lemma [31], which states that a set of $2N_T$ vectors in \mathbb{R}^{N_s} can be mapped into a randomly generated subspace \mathbb{R}^k of dimension $k \sim \mathcal{O}(\log 2N_T / \epsilon^2)$ while preserving all pairwise L_2 norms to within a factor of $(1 \pm \epsilon)$, where $0 < \epsilon < 1$, with a very high probability. Here, ϵ is the mismatch or distortion tolerated in the pairwise L_2 norms between any two filters after projection. Thus, RP also approximately preserves any statistic of the dataset that is characterized by such pairwise distances. The RP of \mathbf{H} onto \mathbb{R}^k produces $\mathbf{H}\mathbf{\Omega}$; the accuracy of this data-oblivious transformation depends on the target dimensions and sampling distribution of the $N_s \times k$ projection matrix $\mathbf{\Omega}$. While it is enough to sample the entries independently and identically distributed from a sub-Gaussian distribution, here we choose them independently from a Gaussian distribution with mean zero and variance $1/k$, i.e., $\mathcal{N}(0, 1/k)$, thus producing a Gaussian quasi-orthonormal random matrix [35, 36] such that $\langle \mathbf{\Omega}\mathbf{\Omega}^T \rangle = \mathbf{I}$. Results obtained from RP-based processing can vary depending on the actual choice of the distribution (from which elements of $\mathbf{\Omega}$ are drawn), and in a statistical sense, these results arising from different choices of $\mathbf{\Omega}$ are expected to be equivalent due to the quasi-orthonormality of the projection, as explained geometrically in Appendix A.

IV. RP-BASED TEMPLATE MATRIX FACTORIZATION

The key idea behind an ℓ -truncated SVD approximation of \mathbf{H} is to reconstruct the rows of the template matrix using the top- ℓ right-singular vectors. This

approximation works well since \mathbf{H} has a fast-decaying spectrum, as shown in Fig. 2. In making the truncation, one effectively reduces \mathbf{H} to its ℓ -rank approximation $\mathbf{H}^{(\ell)}$. Further, for a bank of normalized templates, it is easy to show that the average fractional loss in SNR due to the truncation is given as $\langle \delta\rho/\rho \rangle = \|\mathbf{H} - \mathbf{H}^{(\ell)}\|_F^2 / \|\mathbf{H}\|_F^2$, where $\langle \cdot \rangle$ denotes average over the bank of templates and $\|\cdot\|_F$ is the Frobenius norm [37]. However, the existing SVD algorithms do not scale well with increasing dimensions and redundancies of the template database.

Randomized-SVD (RSVD) [38] is a RP-based matrix-factorization technique to obtain an ℓ -rank matrix factorization $\mathbf{H}^{(\ell)}$ such that, for some specified $\eta > 0$, $\|\mathbf{H} - \mathbf{H}^{(\ell)}\|_F \leq \min_{\{\mathbf{X} : \text{rank}(\mathbf{X}) \leq \ell\}} \|\mathbf{H} - \mathbf{X}\|_F (1 + \eta)$ with high probability. The RSVD algorithm proceeds by first projecting the individual row-vectors in the template matrix \mathbf{H} to \mathbb{R}^ℓ by using $\tilde{\mathbf{\Omega}}_{N_s \times \ell} \in \mathcal{N}(0, 1/\ell)$, thereby yielding $\tilde{\mathbf{H}}_{2N_T \times \ell} = \mathbf{H}\tilde{\mathbf{\Omega}}$. The latter can be used to perform an SVD-like factorization directly in \mathbb{R}^ℓ through a series of operations as described below.

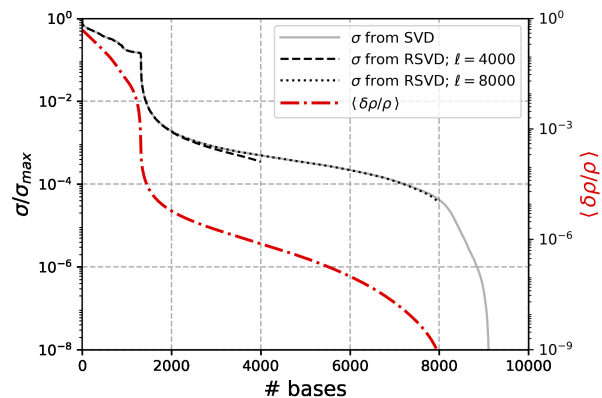


FIG. 2. **Left vertical-axis:** Comparison of singular values σ of the template matrix of size 9130×65536 (normalized by the maximum singular value σ_{max}) as obtained from SVD and RSVD factorization. RSVD is performed in target dimensions \mathbb{R}^ℓ where $\ell = 4000$ or 8000 . The spectrum is seen to fall steeply. This template bank was constructed using non-spinning signal model for component mass parameters ($m_{1,2}$) in the range $2.5M_\odot \leq m_1, m_2 \leq 17.5M_\odot$). There is obviously a trade-off between the desired accuracy and the reduction in the cost and memory to carry out the factorization. As seen from the traces the agreement between the singular values of $\mathbf{H}^{(\ell=4000)}$ is slightly worse than those of $\mathbf{H}^{(\ell=8000)}$ as compared to the singular values of the full template matrix \mathbf{H} .

Right vertical axis: Average SNR reconstruction error as given in Eq. (3) for $\ell = 8000$. As expected, the reconstruction improves with increasing number of basis vectors.

As seen in Fig. 2, it is typically sufficient to take $\ell \ll N_T$. In fact, the numerical value of ℓ chosen in RSVD might be smaller than the theoretical JL bound prescribed for preserving pairwise L_2 distances between the $2N_T$ rows to a η distortion factor.

Working with the reduced sized matrix $\bar{\mathbf{H}}$ leads to significant computational savings, while producing a decomposition that closely approximates the optimal ℓ -rank factorization of \mathbf{H} . It is customary to oversample ℓ by a small factor for better numerical results. This is implicitly assumed below.

RSVD thus proceeds by obtaining a set of orthogonal bases for the column space of $\bar{\mathbf{H}}$ by using a QR decomposition: $\bar{\mathbf{H}} = \mathbf{Q}\mathbf{R}$, where \mathbf{Q} is an orthonormal matrix with dimensions $2N_T \times \ell$. The approximate rank- ℓ decomposition is then obtained as $\mathbf{H}^{(\ell)} = \mathbf{Q}(\mathbf{Q}^T\mathbf{H}) = \mathbf{Q}\mathbf{B}$, where $\mathbf{B}_{\ell \times N_s} \equiv \mathbf{Q}^T\mathbf{H}$ is a matrix that defines the orthonormal projection of the template waveforms into the compressed subspace. It is clear that one can use the ℓ rows of \mathbf{B} as the surrogate templates, which in turn can be used to correlate against the detector data \vec{S} . These can be further combined with \mathbf{Q} to reconstruct ρ in \mathbb{R}^{N_s} . We can thus use the QB decomposition itself to improve the efficiency of both the time and frequency domain searches by constructing \mathbf{H} appropriately, with templates from the corresponding domains.

Instead of randomly projecting the column space of \mathbf{H} , the method can be generalized by applying RP on both the row and column spaces [38]. This bilateral RSVD method is particularly useful when both N_s and N_T are very large. Figure 2 compares the singular values obtained by the RP-based factorization against those from a direct SVD factorization.

V. RECONSTRUCTION OF SNR

The rank- ℓ matrix factorization of \mathbf{H} using RSVD is given by $\mathbf{H}^{(\ell)} = \mathbf{Q}\mathbf{B}$. Thus, the SNR ρ'_α , for any given t_0 , can be reconstructed in \mathbb{R}^{N_s} as

$$\begin{aligned} \rho'_\alpha &= \left(H_{(2\alpha-1)}^{(\ell)} - iH_{(2\alpha)}^{(\ell)} \right) \vec{S}^T \\ &= \sum_{\nu=1}^{\ell} (Q_{(2\alpha-1)\nu} - iQ_{(2\alpha)\nu}) \left(B_\nu \vec{S}^T \right). \end{aligned} \quad (2)$$

Using Pythagoras theorem, and the fact that $\|\mathbf{H}\|_F^2 = 2N_T$, it is easy to show that the average fractional loss of SNR is given by

$$\left\langle \frac{\delta\rho}{\rho} \right\rangle \leq \frac{\|\mathbf{H}\|_F^2 - \|\mathbf{H}^{(\ell)}\|_F^2}{\|\mathbf{H}\|_F^2} = 1 - \frac{\sum_{\mu=1}^{\ell} \sigma_\mu^2}{2N_T}, \quad (3)$$

where σ_μ are the eigenvalues of $\mathbf{H}^{(\ell)}$. For the example discussed in Fig. 2, $\sum_{\mu=1}^{\ell} \sigma_\mu^2 / (2N_T) < 1$ but approaches unity monotonically with increasing ℓ . The right-hand side of Eq. (2) can be calculated efficiently by evaluating the Frobenius norm of \mathbf{B} directly (i.e., without explicitly finding the eigenvalues of $\mathbf{H}^{(\ell)}$ first). Thus, the QB decomposition can indeed serve as a stand-in replacement for the SVD factorization. For an efficient method of explicitly calculating the SVD factors from the RP-based factorization see Appendix B.

Ideally one would like to use $\langle \delta\rho/\rho \rangle$ as the control parameter and solve Eq. (3) for the optimum value of ℓ . However, this is a hard problem and in practice the value is set by a process of trial and error, which thankfully can be done off-line even when the computation in Eq. (2) is conducted on-line.

A. Random projection based correlations

A naive implementation of matched-filter in time-domain can be very expensive, with a complexity of $\mathcal{O}(N_s^2)$ per template for N_s time-shifts. Of course, the Fast Fourier transform can reduce this to $\mathcal{O}(N_s \log N_s)$. It is however more efficient instead to first project the two aforementioned whitened time-series vectors in \mathbb{R}^{N_s} to a random k -dimensional ($k \ll N_s$) subspace and then cross-correlate; the pairwise distance-preserving property of RP guarantees that the matched-filter output in \mathbb{R}^k will be approximately equal to ρ_α in \mathbb{R}^{N_s} (see Appendix C on how FFT-like algorithms enable its fast computation [37]).

VI. COMPUTATIONAL COMPLEXITY ANALYSIS

The straight-forward SVD factorization of \mathbf{H} requires $\mathcal{O}(N_T^2 N_s)$ floating-point operations, assuming $N_T \leq N_s$. In comparison, the cost of the RP matrix factorization is $\mathcal{O}(\ell N_T N_s + (\ell^2 N_T - \frac{2}{3}\ell^3) + \ell N_T N_s + \ell N_s)$. In this last expression, we have included partial contributions from first projecting the template matrix to \mathbb{R}^ℓ , then taking the QR decomposition of $\bar{\mathbf{H}}$ using Householder's method [39], followed by the cost of constructing \mathbf{B} and calculating its Frobenius norm. For practical cases, one expects $\ell \ll N_s$, due to which the cost of factorizing \mathbf{H} can be several orders of magnitude less than a full SVD factorization. This advantage is not just realized off-line, but can also directly impact the total on-line cost of the searches owing to a lower value of ℓ alone: Figure 1 shows that for moderate sized banks one effectively ends up using $\sim 3 - 4$ times fewer surrogate templates in the on-line portion of the search from the new RP-based factorization. This improvement is expected to be higher for larger banks.

For on-line searches, the number of floating point operations per second (flops) in our method is $N_{\text{flops}} = (2\ell k f_s + 2\ell N_T f_s + k f_s)$. The first term is the number of floating-point operations required for computing the cross-correlation between the surrogate templates (rows of \mathbf{B}) and the data vector; the second term is the cost of reconstruction of the SNR for every template; and the third term is the cost of projecting the data vector into the lower-dimensional space. In the SVD-only method, the expression for N_{flops} is analogous, except that instead of the last term above, it has a down-sampling cost that

is similarly insignificant as our projection cost. The primary difference between the two methods is that owing to our use of RSVD and RP, ℓ and k are less than the number of basis templates and the number of time samples of data used, respectively, in the SVD-only method. For the crucial last couple of seconds of the cross-correlation analysis for CBC signals we have evaluated that our method is an order of magnitude faster than the SVD-only method.

In summary, here we introduced random projection-based techniques that hold promise for factorization of large template matrices and cross-correlation of templates with data in a scalable and computationally efficient way, which can aid more complex searches, such as of CBCs with generic spins, and, hence, improve the chances for new discoveries.

ACKNOWLEDGMENTS

We would like to thank Surabhi Sachdev for carefully reading the manuscript and making useful comments. This work is supported in part by DST's SERB grant EMR/2016/007593 and ICPS programs, NSF grant PHY-1506497, and the Navajbai Ratan Tata Trust. A large set of data analysis studies were performed on the Sarathi computing cluster at IUCAA.

Appendix A: Geometric explanation for top singular subspace preservation under RSVD.

Here we provide a geometric explanation behind the statement that RSVD preserves the top singular subspaces. Figure 3 depicts this intuition.

We denote the L_2 norm of a vector as $\|\cdot\|$. Recall that given \mathbf{H} , finding out the top- k singular vectors is akin to the question of finding out orthogonal directions u_1, \dots, u_k such that if $\mathbf{U} = [u_1, \dots, u_k]$, then $\|\mathbf{U}\mathbf{U}^T\mathbf{H}\|_F^2 = \|\mathbf{U}^T\mathbf{H}\|_F^2 = \sum_{i=1}^k \|u_i^T\mathbf{H}\|^2$ is maximized (squared lengths of vectors in subfigure (a)).

Given the length-preserving properties of random projection, the sum of the squared lengths of $u_i^T\mathbf{H}$ is equivalent, up to an approximation factor of $1 \pm \epsilon$, to the sum of squared lengths of $(u_i^T\mathbf{H})\mathbf{\Omega}$ (subfigure (b)), i.e.,

$$(1 - \epsilon) \sum_{i \leq k} \|u_i^T\mathbf{H}\|^2 \leq \sum_{i \leq k} \|(u_i^T\mathbf{H})\mathbf{\Omega}\|^2.$$

Hence, we instead find orthonormal vectors $\{a_1, \dots, a_k\}$ that are the top- k left singular directions of $\mathbf{H}\mathbf{\Omega}$, such that $\sum_{i \leq k} \|a_i^T(\mathbf{H}\mathbf{\Omega})\|^2$ is maximum (subfigure (c)), thus achieving $\sum_{i \leq k} \|a_i^T(\mathbf{H}\mathbf{\Omega})\|^2 \geq \sum_{i \leq k} \|u_i^T\mathbf{H}\|^2$.

Again by using the length preservation of random projection, we have that $\|a_i^T\mathbf{H}\|^2 \geq (1 - \epsilon)\|(a_i^T\mathbf{H})\mathbf{\Omega}\|^2$ (subfigure (d)). Putting the above steps together, we

find

$$\begin{aligned} \sum_{i=1}^k \|a_i^T\mathbf{H}\|^2 &\geq (1 - \epsilon) \sum_{i=1}^k \|(a_i^T\mathbf{H})\mathbf{\Omega}\|^2 \\ &\geq (1 - \epsilon) \sum_{i=1}^k \|(u_i^T\mathbf{H})\mathbf{\Omega}\|^2 \\ &\geq (1 - \epsilon)^2 \sum_{i=1}^k \|u_i^T\mathbf{H}\|^2. \end{aligned} \quad (\text{A1})$$

Recall that by definition of singular vectors, we already have $\sum_{i=1}^k \|a_i^T\mathbf{H}\|^2 \leq \sum_{i=1}^k \|u_i^T\mathbf{H}\|^2$. Let $\mathbf{A} = [a_1, \dots, a_k]$ and recall that $\mathbf{U} = [u_1, \dots, u_k]$. Given that \mathbf{U} is an orthonormal matrix, the matrix $\mathbf{U}\mathbf{U}^T\mathbf{H}$ represents the projection of columns of \mathbf{H} onto the subspace spanned by the columns of \mathbf{U} , and hence is a rank- k approximation of \mathbf{H} . Therefore, it follows from the above argument, that the low rank approximation $\mathbf{A}\mathbf{A}^T\mathbf{H}$ found by RSVD captures most of the energy in the optimal rank- k approximation $\mathbf{U}\mathbf{U}^T\mathbf{H}$.

Appendix B: Calculating the SVD factors from the RP-based factorization efficiently

An efficient method of explicitly calculating the SVD factors from the RP-based factorization is now presented. This is intended as a bridge between the two methods. Singular values can be obtained by performing an SVD on \mathbf{B} , or by first calculating $\mathbf{T}_B = \mathbf{B}\mathbf{B}^T$, of size $\ell \times \ell$. The eigenvectors \mathbf{U}_{T_B} of \mathbf{T}_B are identical to the left-singular vectors of \mathbf{B} , and the eigenvalues $\mathbf{\Sigma}_{T_B}$ are equal to the squares of the singular values of \mathbf{B} . As \mathbf{T}_B is a much more compressed matrix compared to \mathbf{B} , it is far more efficient to store it in memory and factorize it thereby revealing the singular values and left-singular vectors. These in turn can be further used to calculate the singular values of $\mathbf{H}^{(\ell)}$. The top- ℓ right-singular vectors of \mathbf{H} in \mathbb{R}^{N_s} can be obtained using the left-singular vectors of \mathbf{T}_B : $\mathbf{U}_H^{(\ell)} \approx \mathbf{Q}\mathbf{U}_{T_B}$. Similarly, it can be trivially checked that $\mathbf{\Sigma}_H\mathbf{V}_H^T = \mathbf{U}_{T_B}^T\mathbf{B}$. Thus, all the pieces of the SVD factorization of \mathbf{H} can be recovered from RSVD factors, but at a small fraction of the computational cost of the former. In doing so, the advantages of RP-based factorization can be directly transferred to the current SVD-based data analysis pipelines.

Appendix C: Random projection based correlations

A naive implementation of matched-filter in time-domain can be very expensive, with a complexity of $\mathcal{O}(N_s^2)$ per template. Here we show how random projections can be applied to reduce this cost considerably: the whitened time-series vectors, in the form of the template and the data, in \mathbb{R}^{N_s} can be first projected to a random k -dimensional ($k \ll N_s$)

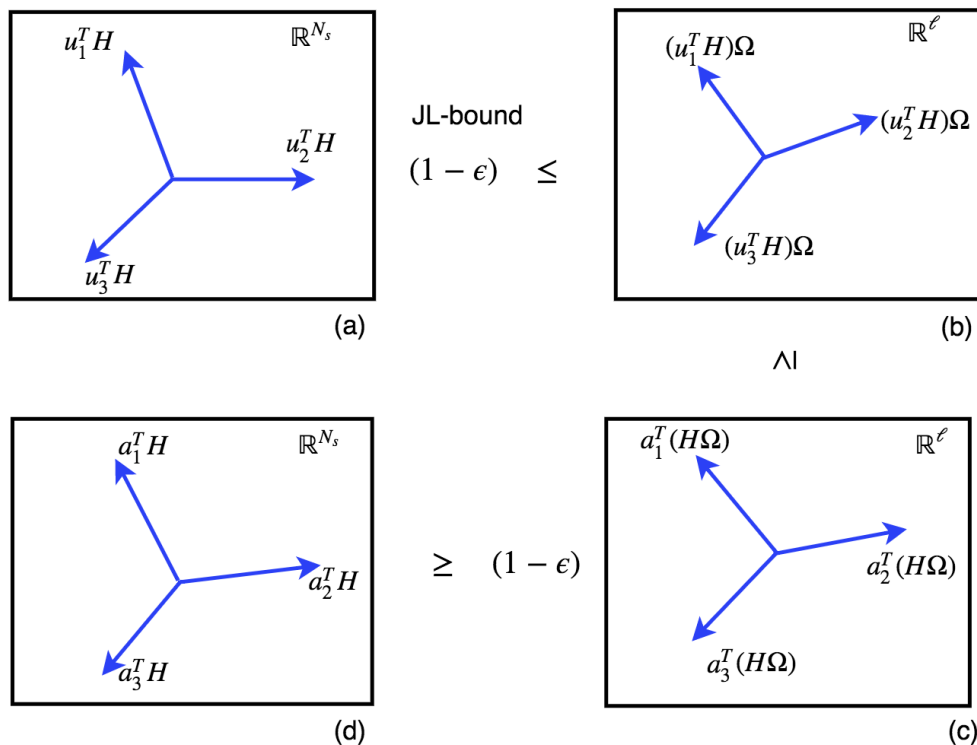


FIG. 3. Depiction of the geometrical intuition behind the preservation of the top singular subspaces in RSVD. Finding the top- k singular vectors for a given \mathbf{H} is akin to the finding the orthogonal directions u_1, \dots, u_k such that the sum of lengths of the vectors $u_i^T \mathbf{H}$ is maximized. Subfigure (a) shows these vectors in the original feature space. Subfigure (b) depicts the action of random projection of these vectors to a lower-dimensional space using the projection matrix Ω . The length-preserving properties of random projections guarantee that the distortion in their lengths lies within a factor of $1 \pm \epsilon$. Subfigure (c) depicts the action of $\mathbf{H}\Omega$ along its top- k left singular directions $\{a_1, \dots, a_k\}$, such that $\sum_{i \leq k} \|a_i^T(\mathbf{H}\Omega)\|^2$ is maximum. Note that these vectors $a_i^T(\mathbf{H}\Omega)$, can also be geometrically interpreted as the the random projection of the vectors $a_i^T \mathbf{H}$ (as shown in subfigure (d) using Ω). Through this chain of subfigures, it follows that the low rank approximation $\mathbf{A}\mathbf{A}^T \mathbf{H}$ found by RSVD captures most of the energy in the optimal rank- k approximation $\mathbf{U}\mathbf{U}^T \mathbf{H}$.

subspace and then cross-correlated; the pairwise distance-preserving property of RP guarantees that the matched-filter output ρ'_α in \mathbb{R}^k will be approximately equal to ρ_α in \mathbb{R}^{N_s} , i.e.,

$$\langle \rho'_\alpha \rangle = \langle (H_{(2\alpha-1)} \Omega - iH_{(2\alpha)} \Omega) (\vec{S} \Omega)^T \rangle = \rho_\alpha,$$

because $\langle \Omega \Omega^T \rangle = I$.

It can also help searches to use the RP-based correlation in conjunction with the RP-based QB factorization of the template matrix described above. The key to this fusion between the two RP-based methods lies in the fact that instead of matched-filtering the data \vec{S} against every template in the bank, one can use the reduced set of $\ell \leq 2N_T$ row vectors of \mathbf{B} as surrogate templates for this purpose. These correlations can be calculated in \mathbb{R}^k by projecting \vec{S} and each row vector $B_\nu \in \mathbb{R}^{N_s}$ to the target k -dimensional subspace. Such projections preserve the inner products between the data and B_ν at every relative time-shift within the ϵ bound, as guaranteed by the JL lemma. The complex SNR for each template can be reconstructed using the coefficient matrix $\mathcal{C}_{N_T \times \ell}$, whose elements are $\mathcal{C}_\alpha \equiv (Q_{(2\alpha-1)\nu} - iQ_{(2\alpha)\nu})$ as shown in the main text.

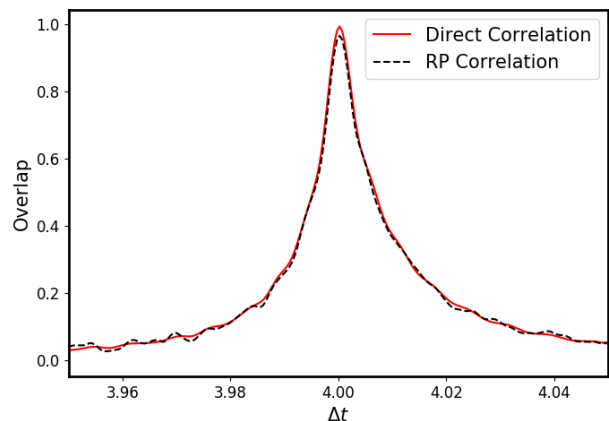


FIG. 4. The phase-maximized overlap time series of a normalized template (corresponding to equal component masses $m_{1,2} = 6 M_\odot$) correlated against a copy of itself time shifted by 4 seconds. The template is taken to be 8 seconds long and sampled at 2048 Hz. The circular correlations are calculated both *directly* in a high dimensional space \mathbb{R}^{N_s} and using RP in a lower dimensional Euclidean space \mathbb{R}^k , as discussed in Appendix C; here $N_s = 16384$ and $k = N_s/2$. The agreement between the two traces show that RP can be used to efficiently calculate overlaps in a lower dimensional space.

The phase-maximized SNRs of the templates are given by the modulus of resulting complex SNRs.

The construction proceeds as follows: Suppose data are sampled at a rate f_s and that the duration in which one decides to search for the signal's time of arrival is τ , which is taken to be longer than the longest template in the bank. Then the number of points over which one is discretely searching for t_0 is $f_s\tau$. We next construct a partial circulant matrix $\mathbf{K}(B_\nu)$ for every row of \mathbf{B} , such that its dimensions are $(f_s\tau) \times (f_s\tau + N_s)$. Its n^{th} row $K_n(B_\nu)$ is a copy of B_ν that is time-shifted by an amount $\Delta t_n = n/f_s$, where $n \in [0, (f_s\tau)]$. The remaining $f_s\tau$ elements in each row are set to zero. The data vector \vec{S} , with $(f_s\tau + N_s)$ time-points, and the circulant matrices can both be randomly projected to the subspace \mathbb{R}^k using $\mathbf{\Omega}$. Their subsequent multiplication is used to construct the cross-correlation:

$$\rho'_\alpha(\Delta t_n) = \sum_\nu C_{\alpha\nu} (K_n(B_\nu) \mathbf{\Omega}) (\vec{S}\mathbf{\Omega})^T, \quad (\text{C1})$$

where α is the index over the templates in the bank $\nu = 1, \dots, \ell$ is the index on the rows of \mathbf{B} , and $\mathbf{\Omega}$ has dimensions of $(f_s\tau + N_s) \times \ell$. A circulant matrix can be diagonalized using FFT-like algorithms to enable efficient processing of matrix-vector products involving such matrices [37].

Appendix D: SNR reconstruction using QB decomposition of the template bank

We have shown above that very large template banks can be efficiently QB decomposed using the RSVD algorithm thereby representing the template matrix by its rank- ℓ approximation. One can reconstruct the SNR time series for each template in this bank to a high degree of accuracy by projecting the data on the top ℓ basis vectors, akin to the truncated SVD paradigm. The average SNR loss can be estimated from the singular values corresponding to the discarded basis vectors.

We now present results from a Monte-Carlo study to explicitly demonstrate that the fractional SNR loss (averaged over the bank) due to the rank- ℓ approximation of the template matrix closely follows the theoretically estimated value, thereby validating the accuracy of the RSVD factorization.

We consider a template bank \mathbf{H} containing $N_T = 581$ templates covering the component mass space: $5 \leq m_{1,2}/M_\odot \leq 15$ using non-spinning TaylorT4 waveforms. For this study, each waveform was taken to be 8 seconds

long, sampled at 2048 Hz, thereby setting $N_s = 16384$. We use the aLIGO Zero Detuned High Power (ZDHP) noise power spectral density [40]. Signals were simulated for 500 CBC sources, with component masses randomly chosen from the aforementioned mass range. These were separately added to colored Gaussian noise with aLIGO

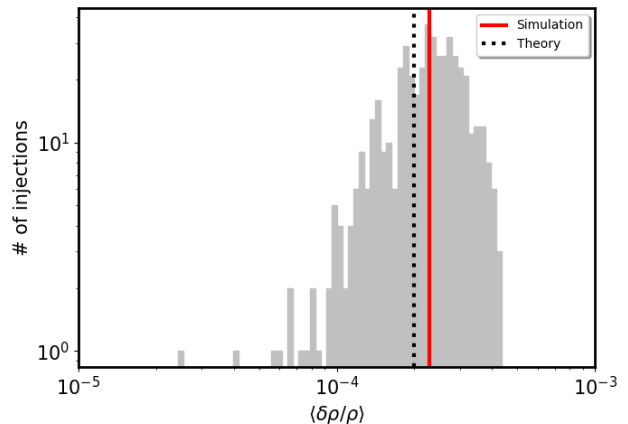


FIG. 5. The distribution of averaged SNR loss summarizing the results of the Monte-Carlo injection study presented in Appendix D. The mean of the distribution (solid red vertical line) is close to the theoretically expected mean loss (dotted black vertical line). The similarity of the results of this study with a similar study presented in Ref. [28] establishes the validity of efficient RP-based QB factorization of the template banks presented in this work.

ZDHP power spectral density. The amplitudes of the injected signals were adjusted for a target SNR of 8.

The template matrix was first QB decomposed to a rank $\ell = 200$ approximation using the RSVD algorithm that corresponded to an averaged SNR loss $\langle \delta\rho/\rho \rangle = \sum_{\ell+1}^{2N_T} \sigma_i^2 = 2 \times 10^{-4}$. This threshold was decided based on the spectrum of the singular values of \mathbf{H} .

For each simulated signal injection, the SNR for every template was reconstructed using the 200 basis vectors and compared with the SNR calculated from a direct circular correlation of these templates against the noisy data containing the injection. Thereafter the averaged SNR loss was evaluated. The distribution of this quantity over the set of all injections is shown in Fig. 5. As shown there, the mean of the distribution agrees well with the target set at 2×10^{-4} . Note that the correlations were computed in \mathbb{R}^{N_s} .

A similar study was presented by Cannon et al. [28] using truncated SVD factorization of the template matrix. The similarity of the results establishes the validity of efficient QB decomposition of large template banks after random projection.

[1] B. P. Abbott *et al.* (Virgo, LIGO Scientific), *Phys. Rev. Lett.* **116**, 061102 (2016), arXiv:1602.03837 [gr-qc].

[2] B. P. Abbott *et al.* (Virgo, LIGO Scientific), *Phys. Rev. Lett.* **116**, 241103 (2016), arXiv:1606.04855 [gr-qc].

- [3] B. P. Abbott *et al.* (Virgo, LIGO Scientific), *Phys. Rev.* **X6**, 041015 (2016), arXiv:1606.04856 [gr-qc].
- [4] B. P. Abbott *et al.* (VIRGO, LIGO Scientific), *Phys. Rev. Lett.* **118**, 221101 (2017), arXiv:1706.01812 [gr-qc].
- [5] B. P. Abbott *et al.* (Virgo, LIGO Scientific), *Phys. Rev. Lett.* **119**, 141101 (2017), arXiv:1709.09660 [gr-qc].
- [6] B. P. Abbott *et al.* (Virgo, LIGO Scientific), *Phys. Rev. Lett.* **119**, 161101 (2017), arXiv:1710.05832 [gr-qc].
- [7] J. Aasi *et al.* (LIGO Scientific), *Class. Quant. Grav.* **32**, 074001 (2015), arXiv:1411.4547 [gr-qc].
- [8] F. Acernese *et al.* (VIRGO), *Class. Quant. Grav.* **32**, 024001 (2015), arXiv:1408.3978 [gr-qc].
- [9] B. P. Abbott *et al.* (Virgo, Fermi-GBM, INTEGRAL, LIGO Scientific), *Astrophys. J.* **848**, L13 (2017), arXiv:1710.05834 [astro-ph.HE].
- [10] B. P. Abbott *et al.*, *Astrophys. J.* **848**, L 12 (2017), arXiv:1710.05833.
- [11] T. Akutsu *et al.* (KAGRA) (2017) arXiv:1710.04823 [gr-qc].
- [12] C. S. Unnikrishnan, *Int. J. Mod. Phys.* **D22**, 1341010 (2013), arXiv:1510.06059 [physics.ins-det].
- [13] J. Rana, A. Singhal, B. Gadre, V. Bhalerao, and S. Bose, *Astrophys. J.* **838**, 108 (2017), arXiv:1603.01689 [astro-ph.IM].
- [14] V. Srivastava, V. Bhalerao, A. P. Ravi, A. Ghosh, and S. Bose, *Astrophys. J.* **838**, 46 (2017), arXiv:1610.07154 [astro-ph.HE].
- [15] S. Ghosh and S. Bose, (2013), arXiv:1308.6081 [astro-ph.HE].
- [16] C. W. Helstrom, *Elements of Signal Detection and Estimation* (Prentice-Hall, Inc., Upper Saddle River, NJ, USA, 1995).
- [17] B. J. Owen, *Phys. Rev.* **D53**, 6749 (1996), arXiv:gr-qc/9511032 [gr-qc].
- [18] B. S. Sathyaprakash and S. V. Dhurandhar, *Phys. Rev.* **D44**, 3819 (1991).
- [19] R. Prix, *Gravitational wave data analysis. Proceedings: 11th Workshop, GWDAW-11, Potsdam, Germany, Dec 18-21, 2006*, *Class. Quant. Grav.* **24**, S481 (2007), arXiv:0707.0428 [gr-qc].
- [20] I. W. Harry, B. Allen, and B. S. Sathyaprakash, *Phys. Rev.* **D80**, 104014 (2009), arXiv:0908.2090 [gr-qc].
- [21] S. Roy, A. S. Sengupta, and N. Thakor, *Phys. Rev.* **D95**, 104045 (2017), arXiv:1702.06771 [gr-qc].
- [22] T. Cokelaer, *Phys. Rev.* **D76**, 102004 (2007), arXiv:0706.4437 [gr-qc].
- [23] B. Abbott *et al.* (LIGO Scientific), *Phys. Rev.* **D78**, 042002 (2008), arXiv:0712.2050 [gr-qc].
- [24] I. W. Harry, A. H. Nitz, D. A. Brown, A. P. Lundgren, E. Ochsner, and D. Keppel, *Phys. Rev.* **D89**, 024010 (2014), arXiv:1307.3562 [gr-qc].
- [25] S. Babak, *Class. Quant. Grav.* **25**, 195011 (2008), arXiv:0801.4070 [gr-qc].
- [26] G. M. Manca and M. Vallisneri, *Phys. Rev.* **D81**, 024004 (2010), arXiv:0909.0563 [gr-qc].
- [27] S. Privitera, S. R. P. Mohapatra, P. Ajith, K. Cannon, N. Fotopoulos, M. A. Frei, C. Hanna, A. J. Weinstein, and J. T. Whelan, *Phys. Rev.* **D89**, 024003 (2014), arXiv:1310.5633 [gr-qc].
- [28] K. Cannon, A. Chapman, C. Hanna, D. Keppel, A. C. Searle, and A. J. Weinstein, *Phys. Rev.* **D82**, 044025 (2010), arXiv:1005.0012 [gr-qc].
- [29] K. Cannon, C. Hanna, and D. Keppel, *Phys. Rev.* **D84**, 084003 (2011), arXiv:1101.4939 [gr-qc].
- [30] K. Cannon *et al.*, *Astrophys. J.* **748**, 136 (2012), arXiv:1107.2665 [astro-ph.IM].
- [31] W. B. Johnson and J. Lindenstrauss, in *Conference in modern analysis and probability (New Haven, Conn., 1982)*, Contemp. Math., Vol. 26 (Amer. Math. Soc., Providence, RI, 1984) pp. 189–206.
- [32] E. Bingham and H. Mannila, in *Proceedings of the seventh ACM SIGKDD international conference on Knowledge discovery and data mining* (ACM, 2001) pp. 245–250.
- [33] C. Messick *et al.*, *Phys. Rev.* **D95**, 042001 (2017), arXiv:1604.04324 [astro-ph.IM].
- [34] K. Cannon *et al.*, *Astrophys. J.* **748**, 136 (2012), arXiv:1107.2665 [astro-ph.IM].
- [35] S. Dasgupta and A. Gupta, *Random Struct. Algorithms* **22**, 60 (2003).
- [36] S. Dasgupta, in *Proceedings of the Sixteenth conference on Uncertainty in artificial intelligence* (Morgan Kaufmann Publishers Inc., 2000) pp. 143–151, arXiv:1301.3849 [cs.LG].
- [37] G. H. Golub and C. F. Van Loan, *Matrix Computations (3rd Ed.)* (Johns Hopkins University Press, Baltimore, MD, USA, 1996).
- [38] N. Halko, P.-G. Martinsson, and J. A. Tropp, *SIAM review* **53**, 217 (2011), arXiv:0909.4061 [math.NA].
- [39] W. H. Press, S. A. Teukolsky, W. T. Vetterling, and B. P. Flannery, *Numerical Recipes 3rd Edition: The Art of Scientific Computing*, 3rd ed. (Cambridge University Press, New York, NY, USA, 2007).
- [40] *Advanced LIGO anticipated sensitivity curves*, Tech. Rep. LIGO-T0900288-v3 (LIGO Scientific Collaboration, <https://dcc.ligo.org/LIGO-T0900288/public>, 2010).